



AI-driven drug repurposing and binding pose meta dynamics identifies novel targets for monkeypox virus

Chirag N. Patel ^{a,b,1}, Raghvendra Mall ^{c,d,*,2}, Halima Bensmail ^{e,*,3}

^a Department of Botany, Bioinformatics and Climate Change Impacts Management, School of Science, Gujarat University, Ahmedabad 380009, India

^b Chemical Biology Laboratory, Center for Cancer Research, National Cancer Institute, National Institute of Health, Frederick, MD 21702, USA

^c Department of Immunology, St. Jude Children's Research Hospital, 262 Danny Thomas Place, Memphis, TN 38105, USA

^d Biotechnology Research Center, Technology Innovation Institute, Abu Dhabi 9639, United Arab Emirates

^e Qatar Computing Research Institute, Hamad Bin Khalifa University, Doha 34110, Qatar

ARTICLE INFO

Article history:

Received 20 September 2022

Received in revised form 28 February 2023

Accepted 5 March 2023

Keywords:

Monkeypox virus

Double-stranded DNA

DeepRepurpose

Deep learning

Molecular docking and binding pose

metadynamics

ABSTRACT

Monkeypox virus (MPXV) was confirmed in May 2022 and designated a global health emergency by WHO in July 2022. MPXV virions are big, enclosed, brick-shaped, and contain a linear, double-stranded DNA genome as well as enzymes. MPXV particles bind to the host cell membrane via a variety of viral-host protein interactions. As a result, the wrapped structure is a potential therapeutic target. DeepRepurpose, an artificial intelligence-based compound-viral proteins interaction framework, was used via a transfer learning setting to prioritize a set of FDA approved and investigational drugs which can potentially inhibit MPXV viral proteins. To filter and narrow down the lead compounds from curated collections of pharmaceutical compounds, we used a rigorous computational framework that included homology modeling, molecular docking, dynamic simulations, binding free energy calculations, and binding pose metadynamics. We identified Elvitegravir as a potential inhibitor of MPXV virus using our comprehensive pipeline.

© 2023 The Authors. Published by Elsevier Ltd on behalf of King Saud Bin Abdulaziz University for Health Sciences. This is an open access article under the CC BY license (<http://creativecommons.org/licenses/by/4.0/>).

Introduction

Monkeypox virus (MPXV), an Orthopoxvirus genus member [1], is a zoonotic virus discovered in 1958 amid outbreaks of a pox-like illness in macaque monkeys held at a Danish research institution and termed as "monkeypox" [2]. The first human case was found in 1970 under enhanced SPX monitoring in the Democratic Republic of the Congo (DRC) [3]. Monkeypox, double-stranded DNA virus, is a member of the Orthopoxvirus genus in the Poxviridae family, and poxviruses have a strong inclination to spread outside of their normal ecological area by infecting a naïve group [4–6]. Monkeypox is clinically almost identical to conventional Variola (SPX) and Vaccinia, smallpox viruses [7]; as a result, since the universal abolition

of smallpox in 1977, much emphasis has been focused on monkeypox as a smallpox-like illness with universal implications [8].

Initially macular, the lesions progress to papules, vesicles, pustules, and, lastly, crusts. Up to 11% of unvaccinated affected people die [9,10]. Transmission occurs by respiratory droplets or direct contact with lesion exudate; however, there is evidence that infection can occur via bite or scratch [11,12]. There are presently no medications approved to treat monkeypox (MPX), and while the smallpox vaccination can give protection, its usage is limited due to safety concerns with a live viral vaccine. As a result, MPX prevention is dependent on limiting human contact with infected wild animals and avoiding viral transmission from person to person [13,14]. Despite this, there are over a thousand confirmed monkeypox cases in the United States, the United Kingdom, and several other European nations as of June 4, 2022 [15,16]. Monkeypox symptoms include flu-like symptoms, fever, lethargy, back pain, headache, and a unique rash [17,18]. The globe is divided into two clades: Central African clade and West African clade. The Central African clade had a case fatality rate of 10.6%, whereas the West African clade had a rate of 3.6% [19].

Monkeypox is an enveloped double-stranded deoxyribonucleic acid (dsDNA) virus that replicates exclusively in the host cell

* Corresponding author at: Department of Immunology, St. Jude Children's Research Hospital, 262 Danny Thomas Place, Memphis, TN 38105, USA.

** Corresponding author.

E-mail addresses: raghvendra.mall@stjude.org (R. Mall), hbensmail@hbku.edu.qa (H. Bensmail).

¹ <http://orcid.org/0000-0003-0777-7720>

² <https://orcid.org/0000-0003-1779-3150>

³ <https://orcid.org/0000-0002-7084-0502>

cytoplasm and belongs to the Orthopoxvirus genus of the Poxviridae family [20]. F13 encodes a VP37 envelope protein [21] that is essential for the formation of enveloped virions (EVs), which include internal EVs (IEVs), cell-associated EVs (CEVs), and external EVs (EEVs) [22]. F13 has a phospholipase motif that is required for the envelopment of intracellular mature virions (IMVs) into virus-modified membranes to produce egress-competent IEVs [23]. IEVs are carried to the cell surface by microtubules after acquiring extra membranes, where their outer membrane fuses with the plasma membrane, exposing CEVs. CEVs remain attached to the cell surface, push into nearby cells through actin tails that grow beneath them, or are released into the extracellular environment as EEVs [24]. As a result, the prevailing opinion is that CEVs mediate virus propagation from cell to cell and that EEVs facilitate virus systemic dispersion inside a host [25]. Therefore, we had chosen F13 envelope protein for the study. Even though MPXV is a DNA virus, it spends its entire life cycle in the cytoplasm of infected cells [26–28]. All the proteins required for viral DNA replication, transcription, virion assembly, and nuclear egress are encoded by the MPXV genome [29,30]. Until 2019, there are no licensed vaccinations or medicines to treat the human monkeypox virus. Dryvax, a smallpox vaccine, has been used to treat both smallpox and monkeypox [31,32].

Tecovirimat is a drug identified through molecular docking by [33,34] for the treatment of monkeypox and has widely been used for treatment of smallpox disease [33]. Recently Dassanayake et al., 2022, [35], the authors screened for six antimicrobial peptides, two phytochemicals and two bacterial metabolites to test for antiviral properties against multiple viruses including monkeypox virus using molecular docking and identified Glycocin F as the only natural biomolecule with high binding affinity to viral surface proteins. In [36], the authors undertake a drug repurposing approach to identify potential inhibitors for vital monkeypox viral proteins using molecular docking and molecular dynamics simulations. The authors [36] identified Tipranavir and Dolutegravir as potential top inhibitors. Furthermore, the authors in [37] use a network pharmacology approach followed by molecular docking to identify Shengma-Gegen decoction (SMGGD) as a potential inhibitor of monkeypox virus through the MAPK signalling pathway.

In this work, we propose a multi-step in-silico pipeline to identify potential inhibitors targeting the Monkeypox envelope protein. We tested 1483 FDA approved and investigational drugs using the DeepRepurpose framework (including 1482 drugs available in DeepRepurpose dataset and Tecoviramt) to identify top compounds which potentially inhibit MPX viral proteins available in Uniprot. We focused on the monkeypox envelope protein F13 (Uniprot id: Q5IXY0) as it is point of entry for infected human cells. Since the structure of any of the viral proteins relevant to monkeypox were not available, we used AlphaFold to obtain the predicted structure of the envelope protein. We then created a homology model and tested its docking, molecular dynamics (MD) and binding pose metadynamics [38]. This *in silico* pipeline resulted in the identification of the most promising and efficient compounds as a starting point for the development of prospective drugs. The docking and MD results verified each other and revealed a strong connection with the experimental data. We also identified the primary interactions involved in molecular recognition and provided suggestions for the development of efficient and selective therapeutic agents [39].

Materials and methods

Artificial Intelligence based DeepRepurpose framework

We used the DeepRepurpose framework proposed in [40] as the platform for transfer learning. The DeepRepurpose framework builds an ensemble of various machine learning models on top of vector representations of the compounds and the viral proteins for

estimating compound-viral protein activities. It uses a vector representations such as molecular fingerprints (MFP) or a teacher-forcing long short-term memory neural network (TF-LSTM) [41]-based embedding vector for compounds concatenated with a convolutional neural network (CNN) [42]-based embedding vector representation for viral proteins [43–46]. This concatenated vector is then passed to state-of-the-art machine learning models such as XGBoost [47] and Support Vector Machines [48,49] to build predictive models. Additionally, the DeepRepurpose framework uses sequence-based representation for compounds (canonical SMILES strings) and viral protein amino-acid sequence representation (primary structure representation) which is provided to end-to-end deep learning models based on CNNs and graph attention networks (GAT) [50]. The DeepRepurpose framework aggregates the activity scores predicted by each of these models by taking an average of the activity values resulting in the final predicted activity for a given compound-viral protein pair.

DeepRepurpose was built using > 60k interactions between > 50k compounds and ~100 viral organisms with the goal of prioritizing compounds (repurposing) for future pandemic-causing viruses. Moreover, in [40], the authors had collected approximately 12,000 clinical-stage or Food and Drug Administration (FDA)-approved small molecules screened for bioactivities against SARS-COV-2 virus in Vero E6 cells. Two thousand, four hundred eighty-three of these compounds were publicly available in a library named REFRAME (<https://reframedb.org/>). In the DeepRepurpose framework, these compounds were then filtered based on the length of their SMILES sequences resulting in a set (S) comprising of 1482 compounds including known antivirals, antibiotics, anticancer and other human investigational compounds [40].

Furthermore, we obtained 11 viral proteins for the novel monkeypox virus whose sequence information was available in Uniprot (<https://www.uniprot.org/>). These included the cell surface-binding protein (Uniprot Id: Q8V4Y0), poxin-schlafen (Uniprot Id: Q8V4S4), Envelope protein F13 (Uniprot Id: Q5IXY0), thymidine kinase (Uniprot Id: P04363), Envelope protein A28 homolog (Uniprot Id: Q8V4U9), Cu-Zn superoxide dismutase like protein (Uniprot Id: Q8V4T3), telomere-binding protein I1 (Uniprot Id: Q8V518), intermediate transcription factor 3 large subunit (Uniprot Id: Q8V4V4), profilin (Uniprot Id: Q8V4T7) and probable host range protein 2 (Uniprot Id: Q8V566). We screened the 1483 compounds from the DeepRepurpose framework including Tecovirimat to prioritize those compounds which had the highest binding affinity against the majority of the viral proteins of the monkeypox virus (Fig. 1).

Homology modeling

The lack of a resolved crystalized structure spurred the development of monkeypox viral models based on a comparison of primary sequences with the closest accessible known structure. UniprotKB [51] entry Q5IXY0 was used to obtain the primary sequence of the monkeypox envelope protein F13 (Fig. 2). Q5IXY0's FASTA sequence was uploaded to ModWeb: A Server for Protein Structure Modeling [52], AlphaFold2 [53] and Robetta server [54]. AlphaFold's inference pipeline and source code are open source and accessible at <https://github.com/deepmind/alphafold>. Then, multiple sequence alignment was performed using UniRef90, MGnify and small BFD databases. Based on the ModWeb analysis, the template with 7E0M, chain A, with 1.79 Å resolution was selected with psiblast with the best scoring model [55]. The predicted model showed the similarity of 1.08 Å with the reference structure and the e-value of 2. Chimera and AlphaFold were used to determine the predicted local distance difference test (pLDDT) of predicted structures, accordingly. Chimera was employed to retrieve these modelled proteins from AlphaFold and assessed their stereochemistry for structural validation using the SAVES v6.0 of Procheck server [56].

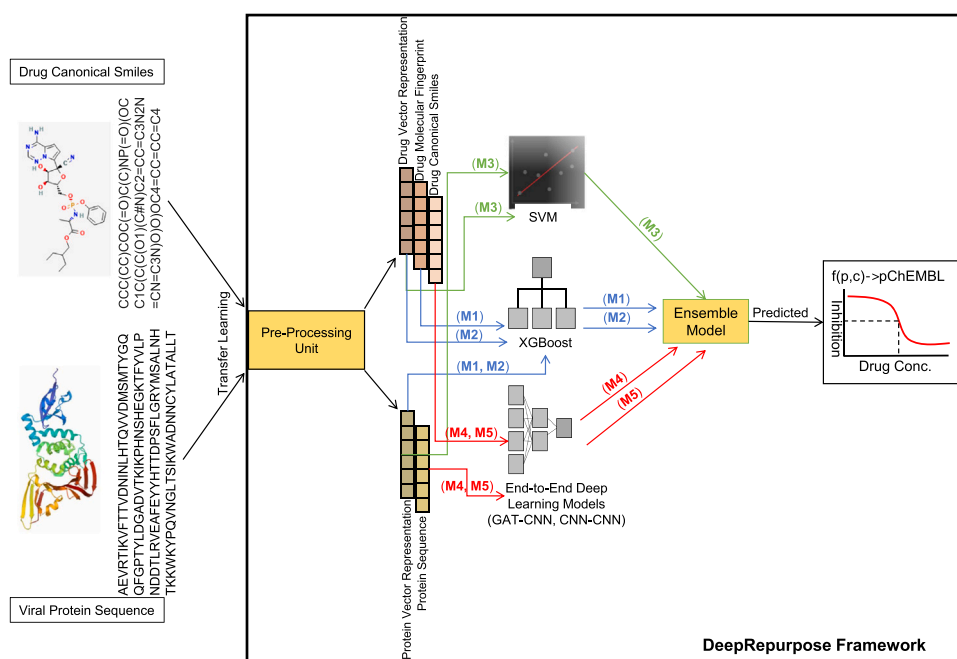


Fig.1. AI-based DeepRepurpose Framework.

>tr[Q5IXY0]Q5IXY0_MONPV Envelope protein F13 OS=Monkeypox virus OX=10244 GN=C19L PE=4 SV=1
 MWPFASVPAGAKRLVETLPENMDFRSDHLTFECNEIITLAKKIYIYIASFCNPLSTTRGALIFDKLK
 EVSEKGIKIVLLDERGKRLGELQSHSPDNFTVVIDKKNNVGLLLGCFWVSDDERCYVGNASTGSSI
 HTIKTLGVSYDYPPLATDLRRRFDTFKAFNSAKNSWNLCSAACCLPVSTAYHIKNPIGGVFVFTDSPELL
 GYSRDLDTVDVIDKLKSAKTSIDIEHLAIVPTTRVDGNSYYWPDYINSIEAAINRGVVKIRLVGNWDKD
 VYSMATARSLDALCVQNDLSVKVFTIQNNKLLIVDDEYVHTSANFDGTHYQNHGFVSNSIDKQLVS
 EAKKIFERDVVSSHSLKLI

Fig.2. Primary sequence of Monkeypox virus envelope F13 protein.

The distribution of amino acid residues derived from Ramachandran plots revealed that 89.9% of the areas were in the most preferred region and 9.2% were in the additional permitted region (Figure S1). This modeled structure was minimized using molecular dynamics simulation for 100 ns for the stabilization.

Molecular docking

The homology modelled protein structure was considered as a receptor and was prepared using the protein preparation wizard of Maestro module of Schrodinger software [57]. It included energy minimization through Optimized Potentials for Liquid Simulations (OPLS) 2005 forcefield [58]. The 1483 AI-based ligands were retrieved from PubChem database (<https://pubchem.ncbi.nlm.nih.gov/>) and prepared for docking by adding charges and hydrogen. These structures were energy minimized and aligned using OPLS 2005 forcefield and greedy algorithm. The homology modeled structure was also prepared using protein preparation wizard of the Schrödinger Glide that includes the addition and removal of the hydrogens using preprocess, and optimization was done through refinement approach aiding the 2005 forcefield [59]. The grid box was built using the pockets detected by sitemap [60] which indicate highest druggability. Therefore, we performed site directed docking. The grid box size was $10 \text{ \AA} \times 10 \text{ \AA} \times 10 \text{ \AA}$. Molecular docking of 1483 AI-based ligands with homology modeled protein was accomplished with increased accuracy utilizing the Glide (grid-based ligand docking with extra precision) software included in the Schrödinger molecular modeling package [61]. The optimal posture for each protein-ligand interaction was determined using the Discovery Studio (DS) visualizer (Accelrys, San Diego, USA). The ligands with the highest

binding energy in the interaction profile were chosen for molecular dynamics simulations [62].

Molecular dynamics simulations

Molecular dynamics (MD) simulations were used to assess the stability of the resultant complexes and the capacity of ligands to bind [63]. In addition to molecular docking, this computational method enables for the investigation of substantial conformational alterations as well as the stabilization of protein-ligand complex [64,65]. Furthermore, it provides a way to determine the binding affinities of the resulting complexes based on the physical motions of atoms and molecules. MD simulations were carried out using the Desmond (Schrödinger Release 2019–3) package [66,67]. For the MD simulation investigation, the docked combination of protein and the top ranked compound identified from molecular docking and was employed for 1 μs time. All receptor-ligand complexes were structurally compliant until they were processed with the protein preparation wizard in the Schrodinger interface [68]. Inserting hydrogens, assigning bonds, and completing incomplete amino acid side chains and loops using hydrogen bond allocation optimization and water orientation sampling (pH 7.0). The periodic simulation box was created using the Machine Builder module with TIP3P (transferable intermolecular potential with three

points) water model and dissolved using OPLS all-atom force field and 1000 iterations of the steepest descent approach for system reduction [69].

After acquiring the equilibrium, the NPT (atoms, pressure, and temperature were kept constant) assembly underwent an uncontrolled development procedure for 1 μs at 300 K and 1.01325 bar. The Nosé-Hoover thermostat and the isotropic Martyna-Tobias-Klein barostat were utilized [70,71]. Short-range (cut-off = 9) and long-range Coulomb interactions were measured using the smooth particle mesh Ewald (PME) system (PME) [72] using a smooth particle network and the RESPA integrator [73]. The system relaxation summary incorporates 1 minimization and 5 equilibration phases with NVT and NPT operations with 1 μs long time period and 5 ps frequency was used to save the configurations. After the simulation, the system's stability was evaluated using a histogram for root mean

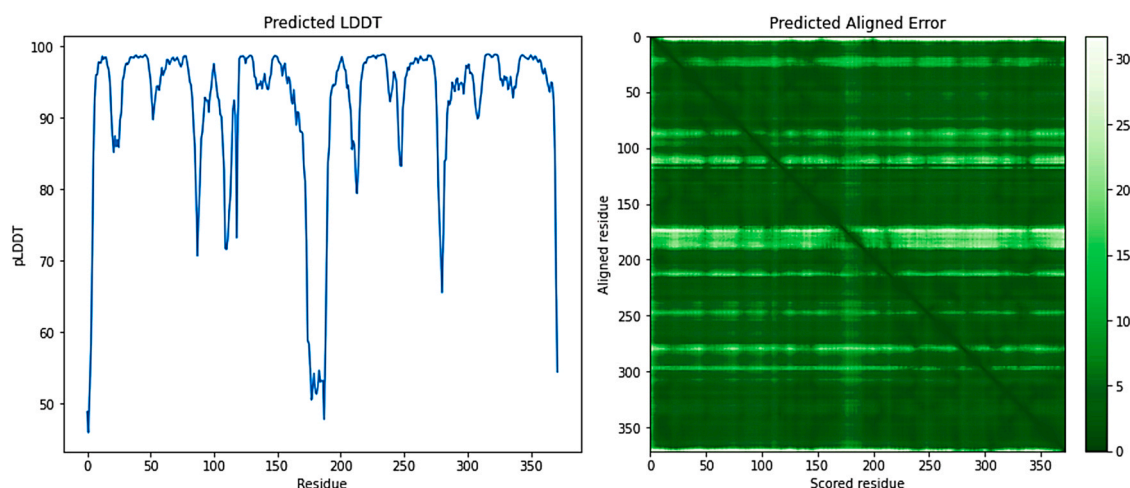


Fig. 3. Homology model confidence score with predicted LDDT and predicted aligned error.

square deviation (RMSD), root mean square fluctuations (RMSF), hydrogen bond analysis, radius of gyration (Rg), and solvent accessible surface area (SASA). Molecular mechanics generalized Born surface area (MM/GBSA) and the single trajectory technique were used to compute the binding free energy [74].

Binding pose metadynamics (BPMD)

BPMD, as implemented in Maestro v.2018.4, is a metadynamics simulation variant in which 10 separate metadynamics simulations of 10 ns are run, using CV as the measure of the ligand heavy atoms' root-mean-square deviation (rmsd) relative to their beginning location. BPMD simulation is a popular improved sampling approach for sampling free energy landscapes [75,76]. For all receptor-ligand complexes binding simulation, biasing collective variables were specified as the distance between the ligand molecule's center of mass and the ligand-binding residues as collective variables (Table 3). According to the RMSD computation, protein residues within 3 Å of the ligands were chosen for alignment. Before computing the heavy atom RMSD to the ligand conformation in the initial frame, the C α s of these binding site residues were linked with those in the initial frame of the binding pose metadynamics trajectory. The hill width and height were set to 0.05 kcal/mol and 0.02 kcal/mol, respectively. Before running the metadynamics, the system was solvated in a box of TIP3P molecules, which was followed by several minimization and restrained MD steps that allowed the system to gradually reach the desired temperature of 300 K while also generating any poor connections and/or strain in the actual starting structure. The essential notion of BPMD was that when subjected to the same biasing force, ligands that were not firmly attached to the receptor would have a greater variation in their RMSD than those that are [75]. BPMD provides three scores that were connected to the ligand's stability during the metadynamics simulations: (1) PoseScore, which was the average RMSD from the initial pose. A rapid increase in the PoseScore indicated that the ligand was not at a well-defined energy minimum and so has not been correctly predicted [77]. (2) PersistenceScore (PersScore) was a measure of hydrogen bond persistence calculated in the last 2 ns of the simulation that contain the same hydrogen bonds as the original structure, averaged across all 10 repeat simulations. Low PersScore was seen in structures whose interaction network is impaired by the BPMD bias. It varies from 0 to 1, with 0 indicating that the ligand had no interactions with the protein at the start and 1 indicating that the interactions between the initial ligand binding mode and the last two ns of the simulations were fully retained [78,79].

Results and discussion

Ligand identification using DeepRepurpose framework

We screened 1483 drugs available in the DeepRepurpose framework for each of 11 viral proteins of MPXV to estimate compound-viral protein activities. DeepRepurpose used end-to-end deep learning models with compound SMILES representation and amino acid sequence of viral proteins as input and generates an activity score as input. Moreover, DeepRepurpose also used vector representations for compounds and viral proteins as input to generate an activity score. The final output of DeepRepurpose was an ensemble of 5 different machine learning models and was the average of the activity scores of these models. The top 20 compounds with the highest average activity across all the 11 viral proteins were highlighted in Supp Table 1. These comprised predominantly of antiviral drugs including Elvitegravir, MK-4965, Triciribine phosphate, Lopinavir and Filociclovir. These drugs were further tested through molecular docking to filter and prioritize the optimal set of drugs against MPXV envelope protein.

Homology modeling

UniprotKB entry Q5IXY0 with 372 amino acids length of monkeypox envelope protein F13 was passed to AlphaFold, Modweb and Robetta servers to get predicted 3D protein structure. We identified that AlphaFold had more accurate predicted structure than other platforms. Modweb and Robetta servers provided structures with low scores in the identification of the template and unreliable z-DOPE score (normalized Discrete Optimized Protein Energy). AlphaFold was employed to compute the predicted Local Distance Difference Test (pLDDT), which indicated the domain accuracy. A pLDDT score greater than 70 suggested high-quality structure. Fig. 3 depicts the mean pLDDT values of predicted protein structure and we can observe that the pLDDT scores were all above 80% for all residues. The pLDDT results showed that the predicted structures were highly accurate. Overall, our findings support AlphaFold's excellent accuracy and dependability in predicting the structure of the envelope protein of the monkeypox virus.

Molecular docking

The homology modelled protein structure was docked with 1483 pharmaceutical compounds. The top five compounds were identified as potential hits for inhibiting the monkeypox viral envelope protein

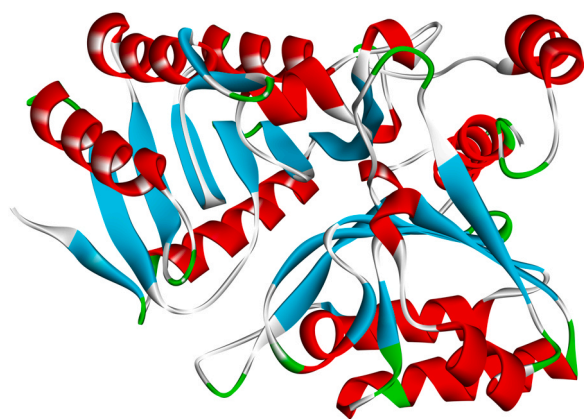
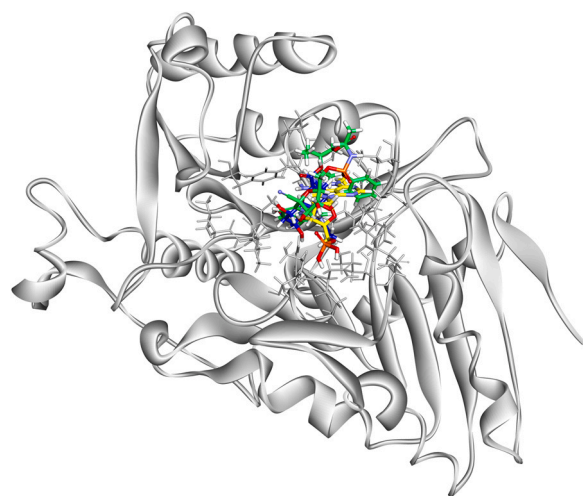


Fig.4. Homology modelled 3D structure of Monkeypox virus envelope F13 protein developed from Alpha fold.



F13 (Fig. 4). According to the binding energy ranking, Elvitegravir has the best binding energy of -5.592 kcal/mol and had 11 H-bonds (with Phe 52, Leu 117, Asn 132, Ser 134, Asn 311, Lys 313, Asn 329 and His 334) (Figure S2). While MK-4965, Triciribine phosphate, Lopinavir and Filiciclovir were described in Figure S3 to Figure S6 with the respective interactions. Table 1 shows the top-ranked compounds with their docking score, XP GScore, glide gscore, glide energy, glide emodel scores and glide energy with the homology modelled protein structure. The electrostatic interactions played a pivotal role in the binding of the monkeypox envelope protein. We have also considered Tecovirimat for docking studies which came in at a very low position with -2.741 kcal/mol score.(Fig. 5,6)

Molecular dynamics (MD) simulations of homology modelled receptor and Elvitegravir

The top-ranked five complexes from the molecular docking experiment were utilized to assess the conformational stability and time-dependent binding capabilities of AI-derived compounds in the homology modelled receptor's catalytic pocket employing molecular dynamic simulations. The MD simulation was run for a time-period of 1 μ s using the Schrodinger Desmond program. To investigate the deviations of ligand binding from its original reference (docked) position, the RMSD measure was used for the conformations

Fig.5. Combined docked posture of top-ranked drugs with Homology modelled structure from the Schrodinger Maestro module's Glide XP docking.

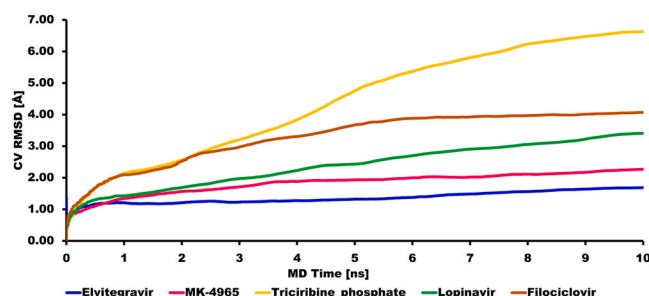


Fig.6. An average RMSD plot of top-5 ranked drugs and Homology modelled structural conformation during 10×10 ns metadynamics runs using PoseScore and PersScore derived values.

Table 1

Docking score and glide binding profiles of the top-21 hits obtained on performing molecular docking.

Sr. No.	Drugs Name	docking score (kcal/mol)	XP GScore (kcal/mol)	glide gscore (kcal/mol)	glide emodel (kcal/mol)	glide energy (kcal/mol)
1	Elvitegravir	-5.456	-5.592	-5.592	-52.978	-40.875
2	MK-4965	-5.429	-5.429	-5.429	-63.597	-46.132
3	Triciribine phosphate	-5.122	-5.212	-5.212	-51.142	-39.932
4	Lopinavir	-5.065	-5.065	-5.065	-69.589	-49.502
5	Filiciclovir	-4.32	-4.32	-4.32	-50.183	-38.818
6	Tipranavir	-3.903	-4.04	-4.04	-68.035	-45.735
7	Zidovudine	-3.736	-3.737	-3.737	-44.097	-33.511
8	BMS-707035	-3.502	-3.503	-3.503	-56.467	-40.378
9	GSK-364735	-3.5	-3.501	-3.501	-55.461	-41.222
10	L-870812	-3.304	-4.207	-4.207	-55.892	-40.512
11	VRT-532	-3.226	-3.594	-3.594	-49.774	-36.029
12	Paritaprevir	-2.635	-2.641	-2.641	-74.653	-55.888
13	PALINAVIR	-2.595	-3.738	-3.738	-117.854	-76.674
14	TMC-647055	-2.366	-2.39	-2.39	-43.477	-29.76
15	Cabotegravir	-2.164	-2.208	-2.208	-49.972	-38.534
16	Simeprevir	-1.668	-1.674	-1.674	-57.947	-39.322
17	ABT-263	-1.588	-3.89	-3.89	-97.968	-66.895
18	Dapivirine	-1.229	-1.229	-1.229	-48.268	-36.137
19	Ritonavir	-1.055	-1.055	-1.055	-83.139	-64.536
20	LM-565	1.791	0.148	0.148	-33.688	-25.491
21	Tecovirimat	-2.741	-2.741	-29.534	-44.063	-40.875

Table 2

MM/GBSA profiles of top-ranked compounds while interacting with the homology modelled protein.

Drugs Name	Binding free energy (kcal/mol)	van der Waals interactions (kcal/mol)	Coulomb Energy (kcal/mol)	Covalent bonding (kcal/mol)	H-bond (kcal/mol)	Lipophilicity (kcal/mol)	Solv_GB (kcal/mol)
Elvitegravir	-45.32	-41.14	-37.97	3.31	-3.24	-13.40	51.82
MK-4965	-39.14	-35.45	-6.03	0.85	-0.46	-14.73	20.51
Triciribine phosphate	-22.47	-27.56	-29.33	3.25	-4.99	-3.39	43.23
Lopinavir	-18.99	-17.71	-6.252	1.39	-0.37	-6.82	11.80
Filiciclovir	-24.83	-26.86	-23.86	7.85	-1.73	-5.32	27.19

Table 3

Selected collective variables from ligand-binding residues for Binding pose metadynamics (BPMD) analysis.

Sr. No.	Drugs Name	Ligand-binding residues
1	Elvitegravir	Leu 239, Asp 283, Asn 312, Lys 314, Ser 327, Asn 329
2	MK-4965	Asn 133, Ser 135, Asn 312, Lys 314, Ser 327, Asn 329
3	Triciribine phosphate	Arg 89, Ser 140, Ile 144, Lys 281, Asn 312, Asn 329
4	Lopinavir	Arg 86, Leu 116, Asn 312, Lys 314, His 334
5	Filiciclovir	Ser 135, Asn 312, Ser 327, His 334

Table 4

Binding Pose Metadynamics analysis of top ranked drugs.

Sr. No.	Drugs Name	Persistence Score	Pose Score
1	Elvitegravir	0.776	1.637
2	MK-4965	0	2.182
3	Triciribine phosphate	0.273	6.461
4	Lopinavir	0	3.234
5	Filiciclovir	0.027	4.015

metric identifies atoms and amino acid residues that have substantial variations over the simulation duration. The RMSF profile of simulated homology modelled receptor complexes attached to Elvitegravir was shown in [Figure S8](#). Met 23, Arg 26, Cys 54, Lys 88, Lys 110, Gly 119, Asn 175, Asn 179, Cys 185, Leu 187, Pro 188, Tyr 214, Val 247, Lys 281 and Ile 372 were noticed with higher fluctuations for all simulated complexes. The radius of gyration (rGyr) of a ligand assessed its 'compactness' and was comparable to its crucial portrayal of stability throughout simulation time. Solvent accessible surface area (SASA) was a measure used to investigate the accessibility of solvent molecules (typically water) to the protein-ligand complex; lower SASA values represent fewer exposure to the soluble environment and the ability of the complex to maintain the hydrophobic core, thereby increasing the overall stability of the complex. [Figure S9](#) and [Figure S10](#) depicted rGyr and SASA properties of all simulated complexes. Among all Elvitegravir, triciribine phosphate and Filiciclovir drugs in the complex with homology modelled receptor possess less variations while MK-4965 and Lopinavir depicts high variations. [Figure S11](#) to [Figure S15](#) shows the intermolecular interactions of all simulated complexes with the homology modelled receptor. In the simulated complexes, Filiciclovir drug produced maximum number of 27 hydrogen bonds and 6 ionic bonds. Whereas Lopinavir made 24 hydrophobic interactions that determined high accountability. Using the MM/GBSA method, total free energy of binding of the top-five drugs was calculated. We have incorporated the interaction profiles of MD simulations at every 100 ns time trajectories to understand the binding mechanism. [Table 2](#) demonstrates the binding free energy calculation observed for all simulated complexes. Elvitegravir secured best binding energy of -45.32 kcal/mol while Lopinavir ranked at last position with the binding energy of -18.99 kcal/mol. This finding demonstrates that Elvitegravir created improved crystal connections as well as new contacts, obtaining the top rank energy between all identified

compounds. Elvitegravir aids to the development of a novel ligand binding theory. In 4-oxo-1,4-dihydropyridine pocket, π -stack with Trp 279 residues and π -alkyl or broadly hydrophobic interactions. It was discovered that hydrogen bonding with Ala 134, Ser 135, Ser 140, and Asn 312 was helpful. MK-4965 came in second with a binding energy of -39.14 kcal/mol owing to novel contacts formed during docking and dynamics simulations. Filiciclovir and Triciribine phosphate came in third and fourth place, respectively. According to MM/GBSA score, lopinavir has the maximum binding energy of -18.99 kcal/mol.

Binding pose metadynamics (BPMD)

The trajectories of all simulated complexes were evaluated to investigate the binding kinetics of the receptor. The metadynamics simulations were carried out using the collective variable listed in [Table 3](#). The PoseScore, which was the RMSD of the ligand with respect to the initial ligand heavy atoms coordinates, was used to determine posture stability. A PoseScore of 2 was seen as steady. Furthermore, the PersScore, which indicated the strength of the hydrogen bonds established between the ligand and the protein residues, was used to examine the data. It was deemed an indication of strong persistence if 60% of the total hydrogen bonds were preserved during the simulations. The homology modelled receptor and all simulated complexes were employed to BPMD protocol. The PoseScore for Elvitegravir was 1.6 Å with lower RMSD range which suggested that it managed to generate strong and consistent hydrogen bond network during the simulations. However, MK-4965 and Lopinavir notified with 2.1 Å and 3.2 Å, respectively. Filiciclovir listed with 4 Å and Triciribine phosphate occupied 6.4 Å PoseScore which were considered as a higher RMSD range. The PersScore was also identified with the value of 0.7 Å which was very significant for the ligand binding stability and lower structural variability. Overall, BPMD showed strong capacity to detect Elvitegravir and additional investigation of the findings gave some insights into conditions that might be hard for the approach. Rest of the drugs possessed the PersScore under the 0.2 Å ([Table 4](#)). As a result, the reference structure for BPMD was not the input structure, but the equilibrated one, which might differ dramatically in some circumstances. Given this discovery, the PoseScore was analyzed to the RMSD with reference equilibrated structure, which was referred to as the MD-RMSD. The goal was to see if unstable postures might be detected ahead of time by the MD equilibration technique. To discover the best approach for balancing accuracy and computational efficiency, a

detailed examination of MD versus BPMD in detecting dubious crystal structures is necessary.

Conclusion

The lack of a suitable medical therapy or vaccine has indeed worsened the situation of a MPXV. Targeting envelope receptor was a key strategy for designing effective inhibitors powered by computer-aided drug design strategies at the first stage of viral invasion as the disease progression is triggered by major contacts between human membrane and envelope proteins. Using a dynamic framework consisting of AI-driven screening, molecular dynamic modeling, free energy binding measurements and binding pose dynamics, this study optimized lead compounds against the homology modelled F13 envelope protein of monkeypox virus. Elvitegravir was found as potential drug candidate with a higher binding affinity score. Both docked complexes were subjected to 1 μ s molecular dynamic simulations, demonstrating the structural stability of protein-ligand complexes. Various measuring techniques, such as RMSD, RMSF, gyration radius, and surface area measurements contributed to the complex's structural integrity. The binding free energy of the Elvitegravir was also measured using MM/GBSA tests, showing that associations with adjacent hydrophobic binding sites of the ligand-binding assist enhanced the binding free energy, while retaining key receptor interactions.

Our *in silico* pipeline provides a computer-aided drug screening approach by reducing the search space through DeepRepurpose followed by homology modelling, molecular docking, molecular dynamics simulations and binding pose metadynamics to identify the optimal set of drugs for MPXV. By using our pipeline, we narrowed down the compound search space to identify, Elvitegravir as a potential compound against MPXV whose efficacy should further be validated through in-vitro and in-vivo experiments.

CRediT authorship contribution statement

C.N.P. and R.M. conceptualized and designed the project. C.N.P. and R.M. developed methodology. C.N.P. and R.M. acquired data. C.N.P. analyzed and interpreted data. C.N.P., R.M. and H.B. wrote manuscript. H.B. provided executive support. C.N.P., R.M. and H.B. supervised the study. The whole manuscript was approved by all authors.

Conflicts of Interest

The authors declare that there are no conflicts of interest.

Acknowledgment

The content is solely the responsibility of the authors and does not necessarily represent the official views of the National Institutes of Health. We acknowledge that the open access funding is provided by the Qatar National Library.

Author approvals

All authors have seen and approved the manuscript, and that it hasn't been accepted or published elsewhere.

Appendix A. Supporting information

Supplementary data associated with this article can be found in the online version at doi:10.1016/j.jiph.2023.03.007.

References

- [1] Alakunle E, Moens U, Nchinda G, Okeke MI. Monkeypox virus in Nigeria: infection biology, epidemiology, and evolution. Vol 12, Page 1257 2020 Viruses 2020;12:1257. <https://doi.org/10.3390/V12111257>
- [2] Bragazzi NL, Kong JD, Mahroum N, Tsigalou C, Khamisy-Farah R, Converti M, et al. Epidemiological trends and clinical features of the ongoing monkeypox epidemic: a preliminary pooled data analysis and literature review. J Med Virol 2022. <https://doi.org/10.1002/JMV.27931>
- [3] Lloyd-Smith JO. Vacated niches, competitive release and the community ecology of pathogen eradication. Philos Trans R Soc B Biol Sci 2013;368. <https://doi.org/10.1098/RSTB.2012.0150>
- [4] Sale TA, Melski JW, Stratman EJ. Monkeypox: an epidemiologic and clinical comparison of African and US disease. J Am Acad Dermatol 2006;55:478–81. <https://doi.org/10.1016/j.jaad.2006.05.061>
- [5] Kabuga AI, El Zowalaty ME. A review of the monkeypox virus and a recent outbreak of skin rash disease in Nigeria. J Med Virol 2019;91:533–40. <https://doi.org/10.1002/JMV.25348>
- [6] Kerr PJ. Myxomatosis in Australia and Europe: a model for emerging infectious diseases. Antivir Res 2012;93:387–415. <https://doi.org/10.1016/j.antiviral.2012.01.009>
- [7] Expunging Variola: The Control and Eradication of Smallpox in India, 1947–1977 - Sanjoy Bhattacharya - Google Books n.d. ([https://books.google.co.in/books?hl=en&lr=&id=Kx2919wvT4C&oi=fnd&pg=PR8&dq=Monkeypox+is+clinically+almost+identical+to+conventional+Variola+\(SPX\)+and+Vaccinia,+smallpox+viruses&ots=y5m5jZVGT9&sig=Sc538HxZRE_QE8yIsfPneHFSq8#v=onepage&q&f=false](https://books.google.co.in/books?hl=en&lr=&id=Kx2919wvT4C&oi=fnd&pg=PR8&dq=Monkeypox+is+clinically+almost+identical+to+conventional+Variola+(SPX)+and+Vaccinia,+smallpox+viruses&ots=y5m5jZVGT9&sig=Sc538HxZRE_QE8yIsfPneHFSq8#v=onepage&q&f=false)) (Accessed August 22, 2022).
- [8] Voigt EA, Kennedy RB, Poland GA. Defending against smallpox: a focus on vaccines. 2016;15:1197–211. <https://doi.org/10.1080/14760584.2016.1175305> (<https://doi.org/10.1080/14760584.2016.1175305>).
- [9] Moore ZS, Seward JF, Lane JM. Smallpox. Lancet 2006;367:425–35. [https://doi.org/10.1016/S0140-6736\(06\)68143-9](https://doi.org/10.1016/S0140-6736(06)68143-9)
- [10] Suarez VR, Hankins GDV. Smallpox and pregnancy: from eradicated disease to bioterrorist threat. Obstet Gynecol 2002;100:87–93. [https://doi.org/10.1016/S0029-7844\(02\)02048-3](https://doi.org/10.1016/S0029-7844(02)02048-3)
- [11] Kumar N, Acharya A, Gendelman HE, Byrareddy SN. The 2022 outbreak and the pathobiology of the monkeypox virus. J Autoimmun 2022;131:102855. <https://doi.org/10.1016/j.jaut.2022.102855>
- [12] Nolen LD, Osadebe L, Katomba J, Likofata J, Mukadi D, Monroe B, et al. Introduction of monkeypox into a community and household: risk factors and zoonotic reservoirs in the Democratic Republic of the Congo. Am J Trop Med Hyg 2015;93:410. <https://doi.org/10.4269/AJTMH.15-0168>
- [13] Brown K, Leggat PA. Human monkeypox: current state of knowledge and implications for the future. Vol 1, Page 8 Trop Med Infect Dis 2016 2016;1:8. <https://doi.org/10.3390/TROPICALMED1010008>
- [14] Reynolds MG, Doty JB, McCollum AM, Olson VA, Nakazawa Y. Monkeypox re-emergence in Africa. a Call Expand Concept Pract One Health 2019;17:129–39. <https://doi.org/10.1080/14787210.2019.1567330>
- [15] Iñigo Martínez J, Gil Montalbán E, Jiménez Bueno S, Martín Martínez F, Nieto Juliá A, Sánchez Díaz J, et al. Monkeypox outbreak predominantly affecting men who have sex with men, Madrid, Spain, 26 April to 16 June 2022. Eur Surveill 2022;27:2200471. <https://doi.org/10.2807/1560-7917.ES.2022.27.22.2200471/CITE/PLAINTEXT>
- [16] Cimerman S, Chebabo A, Cunha CA, da, Barbosa AN, Rodríguez-Morales AJ. Human monkeypox preparedness in Latin America – are we ready for the next viral zoonotic disease outbreak after COVID-19? Brazilian. J Infect Dis 2022;26:102372. <https://doi.org/10.1016/j.bjid.2022.102372>
- [17] Sah R, Abdelaal A, Reda A, Katamesh BE, Manirambona E, Abdelmonem H, et al. Monkeypox and its possible sexual transmission: where are we now with its evidence? Vol 11, Page 924 Pathog 2022 2022;11:924. <https://doi.org/10.3390/PATHOGENS11080924>
- [18] Uwishema O, Adekunbi O, Peñamante CA, Bekele BK, Khoury C, Mhanna M, et al. The burden of monkeypox virus amidst the Covid-19 pandemic in Africa: a double battle for Africa. Ann Med Surg 2022;80:104197. <https://doi.org/10.1016/j.amsu.2022.104197>
- [19] Xiang Y, White A. Monkeypox virus emerges from the shadow of its more infamous cousin. <https://doi.org/10.1080/2222175120222095309> Fam Biol Matters 2022;1–14. <https://doi.org/10.1080/22221751.2022.2095309>
- [20] Khani E, Afsharirad B, Entezari-Maleki T. Monkeypox treatment: current evidence and future perspectives. J Med Virol 2023;95. <https://doi.org/10.1002/JMV.28229>
- [21] Sung TC, Roper RL, Zhang Y, Rudge SA, Temel R, Hammond SM, et al. Mutagenesis of phospholipase D defines a superfamily including a trans-Golgi viral protein required for poxvirus pathogenicity. EMBO J 1997;16:4519–30. <https://doi.org/10.1093/EMBOJ/16.15.4519>
- [22] Petersen B.W., Damon I.K. Orthopoxviruses: Vaccinia (Smallpox Vaccine), Variola (Smallpox), Monkeypox, and Cowpox n.d.
- [23] Chung C-S, Chen C-H, Ho M-Y, Huang C-Y, Liao C-L, Chang W. Vaccinia virus proteome: identification of proteins in vaccinia virus intracellular mature virion particles. J Virol 2006;80:2127–40. <https://doi.org/10.1128/JVI.80.5.2127-2140.2006/ASSET/0201D4B3-EC65-4573-878E-86381D992240/ASSETS/GRAPHIC/ZJV0050674390002.JPEG>
- [24] Sodeik B, Krijnse-Locker J. Assembly of vaccinia virus revisited: de novo membrane synthesis or acquisition from the host? Trends Microbiol 2002;10:15–24. [https://doi.org/10.1016/S0966-842X\(01\)02256-9](https://doi.org/10.1016/S0966-842X(01)02256-9)

- [25] Burckhardt CJ, Greber UF. Virus movements on the plasma membrane support infection and transmission between cells. *PLOS Pathog* 2009;5:e1000621. <https://doi.org/10.1371/JOURNAL.PPAT.1000621>
- [26] Shchelkunov S, Totmenin A, Kolosova I. Species-specific differences in organization of orthopoxvirus Kelch-Like proteins. 2002 242 *Virus Genes* 2002;24:157–62. <https://doi.org/10.1023/A:1014524717271>
- [27] Mok H.G.W. Vaccinia virus requires heat-shock proteins for genome replication and virion assembly. Dr Thesis, UCL (University Coll London) 2019.
- [28] Saxena SK, Ansari S, Maurya VK, Kumar S, Jain A, Paweska JT, et al. Re-emerging human monkeypox: a major public-health debacle. *J Med Virol* 2022. <https://doi.org/10.1002/JMV.27902>
- [29] Sivan G, Weisberg AS, Americo JL, Moss B. Retrograde transport from early endosomes to the trans-Golgi network enables membrane wrapping and egress of vaccinia virus virions. *J Virol* 2016;90:8891–905. <https://doi.org/10.1128/JVI.01114-16/ASSET/4A4DA095-038F-4021-90FF-21CD9AB38181/ASSETS/GRAPHIC/ZJV9991819830009.JPEG>
- [30] Van Vliet K, Mohamed MR, Zhang L, Villa NY, Werden SJ, Liu J, et al. Poxvirus proteomics and virus-host protein interactions. *Microbiol Mol Biol Rev* 2009;73:730–49. <https://doi.org/10.1128/MMBR.00026-09/ASSET/53B3968C-5468-4D61-8B3D-975E9DFBFA00/ASSETS/GRAPHIC/ZMR0040922310002.JPEG>
- [31] Edghill-Smith Y, Golding H, Manischewitz J, King LR, Scott D, Bray M, et al. Smallpox vaccine-induced antibodies are necessary and sufficient for protection against monkeypox virus. 2005 117 *Nat Med* 2005;11:740–7. <https://doi.org/10.1038/nm1261>
- [32] Earl PL, Americo JL, Wyatt LS, Eller LA, Whitbeck JC, Cohen GH, et al. Immunogenicity of a highly attenuated MVA smallpox vaccine and protection against monkeypox. *Nat* 2004 428:6979 2004;428:182–5. <https://doi.org/10.1038/nature02331>
- [33] Sherwat A, Brooks JT, Birnkrant D, Kim P. Tecovirimat and the treatment of monkeypox - past, present, and future considerations. *N Engl J Med* 2022. https://doi.org/10.1056/NEJMP2210125/SUPPL_FILE/NEJMP2210125_DISCLOSURES.PDF
- [34] Sharma V, Panwar A, Garg VK, Tuli HS, Datta S, Sharma AK, et al. Tecovirimat as a potential bioavailable inhibitor against MPXVgp158 established through molecular dynamic simulations and docking studies. *J Pure Appl Microbiol* 2022;16:3168–78. <https://doi.org/10.22207/JPAM.16.SPL1.13>
- [35] Dassanayake MK, Khoo TJ, Chong CH, Di Martino P. Molecular docking and in-silico analysis of natural biomolecules against Dengue, Ebola, Zika, SARS-CoV-2 variants of concern and monkeypox virus. *Int J Mol Sci* 2022;23. <https://doi.org/10.3390/ijms231911131>
- [36] Sahoo AK, Augusthian PD, Muralitharan I, Vivek-Ananth RP, Kumar K, Kumar G, et al. In silico identification of potential inhibitors of vital monkeypox virus proteins from FDA approved drugs. *Mol Divers* 2022;1:1–16. <https://doi.org/10.1007/S11030-022-10550-1/FIGURES/8>
- [37] Dai L, Zhang G, Wan X. Network pharmacology and molecular docking analysis reveal insights into the molecular mechanism of shengma-gegen decoction on monkeypox. *Pathog* 2022;11:1342. <https://doi.org/10.3390/PATHOGENS11111342>
- [38] Patel CN, Jani SP, Jaiswal DG, Kumar SP, Mangukia N, Parmar RM, et al. Identification of antiviral phytochemicals as a potential SARS-CoV-2 main protease (Mpro) inhibitor using docking and molecular dynamics simulations. *Sci Rep* 2021;11:1–13. <https://doi.org/10.1038/s41598-021-99165-4>
- [39] Chowdhury KH, Chowdhury MR, Mahmud S, Tareq AM, Hanif NB, Banu N, et al. Drug repurposing approach against novel coronavirus disease (COVID-19) through virtual screening targeting SARS-CoV-2 main protease. *Page 2* 2020;10:2 *Biol* 2021;Vol 10. <https://doi.org/10.3390/BIOLOGY10010002>
- [40] Mall R, Elbasir A, Almeer H, Islam Z, Kolatkar PR, Chawla S, et al. A modeling framework for embedding-based predictions for compound-viral protein activity. *Bioinformatics* 2021;37:2544–55. <https://doi.org/10.1093/BIOINFORMATICS/BTAB130>
- [41] Lamb AM, Alias Parth Goyal AG, Zhang Y, Zhang S, Courville AC, Bengio Y, et al. Forcing: a new algorithm for training recurrent networks. *Adv Neural Inf Process Syst* 2016;29.
- [42] Lecun Y, Bengio Y, Hinton G. Deep learning. *Nat* 2015 521:7553 2015;521:436–44. <https://doi.org/10.1038/nature14539>
- [43] Rawi R, Mall R, Kunji K, Shen CH, Kwong PD, Chuang GY. ParSnpP: sequence-based protein solubility prediction using gradient boosting machine. *Bioinformatics* 2018;34:1092–8. <https://doi.org/10.1093/BIOINFORMATICS/BTX662>
- [44] Khurana S, Rawi R, Kunji K, Chuang GY, Bensmail H, Mall R. DeepSol: a deep learning framework for sequence-based protein solubility prediction. *Bioinformatics* 2018;34:2605–13. <https://doi.org/10.1093/BIOINFORMATICS/BTY166>
- [45] Elbasir A, Mall R, Kunji K, Rawi R, Islam Z, Chuang GY, et al. BCrystal: an interpretable sequence-based protein crystallization predictor. *Bioinformatics* 2020;36:1429. <https://doi.org/10.1093/BIOINFORMATICS/BTZ762>
- [46] Elbasir A, Moovarkumudalvan B, Kunji K, Kolatkar PR, Mall R, Bensmail H. DeepCrystal: a deep learning framework for sequence-based protein crystallization prediction. *Bioinformatics* 2019;35:2216–25. <https://doi.org/10.1093/BIOINFORMATICS/BTY953>
- [47] Chen T, Guestrin C. XGBoost: A Scalable Tree Boosting System. *Proc 22nd ACM SIGKDD Int Conf Knowl Discov Data Min* n.d. <https://doi.org/10.1145/2939672>
- [48] Cortes C, Vapnik V, Saitta L. Support-vector networks. 1995 203 *Mach Learn* 1995;20:273–97. <https://doi.org/10.1007/BF00994018>
- [49] Mall R, Suykens JAK. Very sparse LSSVM reductions for large-scale data. *IEEE Trans Neural Netw Learn Syst* 2015;26:1086–97. <https://doi.org/10.1109/TNNLS.2014.2333879>
- [50] Veličković Veličković P, Cucurull G, Casanova A, Romero A, Li P, Bengio Y. Graph Atten Netw 2018. <https://doi.org/10.17863/CAM.48429>
- [51] Boutet E, Lieberherr D, Tognolli M, Schneider M, Bairoch A. UniProtKB/Swiss-Prot Plant Bioinforma 2007;89–112. https://doi.org/10.1007/978-1-59745-535-0_4/COVER
- [52] Eswar N, John B, Mirkovic N, Fiser A, Ilyin VA, Pieper U, et al. Tools for comparative protein structure modeling and analysis. *Nucleic Acids Res* 2003;31:3375–80. <https://doi.org/10.1093/NAR/GKG543>
- [53] Cramer P. AlphaFold2 and the future of structural biology. 2021 289 *Nat Struct Mol Biol* 2021;28:704–5. <https://doi.org/10.1038/s41594-021-00650-1>
- [54] Kim DE, Chivian D, Baker D. Protein structure prediction and analysis using the Robetta server. *Nucleic Acids Res* 2004;32:W526–31. <https://doi.org/10.1093/NAR/GKH468>
- [55] Wang F, Liu S, Mao X, Cui R, Yang B, Wang Y. Crystal structure of a phospholipase D from the plant-associated bacteria serratia plymuthica strain AS9 reveals a unique arrangement of catalytic pocket. *Vol 22* 2021 *Int J Mol Sci* 2021;22:3219. <https://doi.org/10.3390/IJMS22063219>
- [56] Tables I. *Int Tables Crystallogr* 2006;2006:722–5.
- [57] Rolta R, Yadav R, Salaria D, Trivedi S, Imran M, Sourirajan A, et al. In silico screening of hundred phytochemicals of ten medicinal plants as potential inhibitors of nucleocapsid phosphoprotein of COVID-19: an approach to prevent virus assembly. *J Biomol Struct Dyn* 2021;39:7017–34. https://doi.org/10.1080/07391102.2020.1804457/SUPPL_FILE/TBSD_A_1804457_SM5451.DOCX
- [58] Jorgensen WL, Maxwell DS, Tirado-Rives J. Development and testing of the OPLS all-atom force field on conformational energetics and properties of organic liquids. *J Am Chem Soc* 1996;118:11225–36. https://doi.org/10.1021/JA9621760/SUPPL_FILE/JA11225.PDF
- [59] Banks JL, Beard HS, Cao Y, Cho AE, Damm W, Farid R, et al. Integrated modeling program, applied chemical theory (IMPACT). *J Comput Chem* 2005;26:1752. <https://doi.org/10.1002/JCC.20292>
- [60] Halgren T. New method for fast and accurate binding-site identification and analysis. *Chem Biol Drug Des* 2007;69:146–8. <https://doi.org/10.1111/j.1747-0285.2007.00483.x>
- [61] Friesner RA, Banks JL, Murphy RB, Halgren TA, Klicic JJ, Mainz DT, et al. Glide: a new approach for rapid, accurate docking and Scoring. 1. Method and assessment of docking accuracy. *J Med Chem* 2004;47:1739–49. <https://doi.org/10.1021/jm0306430>
- [62] Patel CN, Goswami D, Jaiswal DG, Parmar RM, Solanki HA, Pandya HA. Pinpointing the potential hits for hindering interaction of SARS-CoV-2 S-protein with ACE2 from the pool of antiviral phytochemicals utilizing molecular docking and molecular dynamics (MD) simulations. *J Mol Graph Model* 2021;105:107874. <https://doi.org/10.1016/J.JMGM.2021.107874>
- [63] Jorgensen WL, Tirado-Rives J. The OPLS [optimized potentials for liquid simulations] potential functions for proteins, energy minimizations for crystals of cyclic peptides and crambin. *Undefined* 1988;110:1657–66. <https://doi.org/10.1021/JA00214A001>
- [64] Ryabov VA. Constant pressure–temperature molecular dynamics on a torus. *Phys Lett A* 2006;359:61–5. <https://doi.org/10.1016/J.PHYSLETA.2006.05.078>
- [65] Braga C, Travis KP. A configurational temperature Nosé–Hoover thermostat. *J Chem Phys* 2005;123:134101. <https://doi.org/10.1063/1.2013227>
- [66] Marsili S, Signorini GF, Chelli R, Marchi M, Procacci P. ORAC: a molecular dynamics simulation program to explore free energy surfaces in biomolecular systems at the atomistic level. *J Comput Chem* 2010;31:1106–16. <https://doi.org/10.1002/JCC.21388>
- [67] Essmann U, Perera L, Berkowitz ML, Darden T, Lee H, Pedersen LG. A smooth particle mesh Ewald method. *J Chem Phys* 1995;103:8577–93. <https://doi.org/10.1063/1.470117>
- [68] Patel C.N., Goswami D., Sivakumar K., Pandya H.A. Repurposing of anticancer phytochemicals for identifying potential fusion inhibitor for SARS-CoV-2 using molecular docking and molecular dynamics (MD) simulations 2021. <https://doi.org/10.1080/07391102.2021.1902393>
- [69] Patel CN, Jani SP, Jaiswal DG, Kumar SP, Mangukia N, Parmar RM, et al. Identification of antiviral phytochemicals as a potential SARS-CoV-2 main protease (Mpro) inhibitor using docking and molecular dynamics simulations. *Sci Rep* 2021 111 2021;11:1–13. <https://doi.org/10.1038/s41598-021-99165-4>
- [70] Massova I, Kollman PA. Combined molecular mechanical and continuum solvent approach (MM-PBSA/GBSA) to predict ligand binding. *Perspect Drug Disco Des* 2000;18:113–35. <https://doi.org/10.1023/A:1008763014207>
- [71] Wang W, Donini O, Reyes CM, Kollman PA. Biomolecular simulations: Recent developments in force fields, simulations of enzyme catalysis, protein-ligand, protein-protein, and protein-nucleic acid noncovalent interactions. *Annu Rev Biophys Biomol Struct* 2001;30:211–43. <https://doi.org/10.1146/annurev.biophys.30.1.211>
- [72] Wang J, Hou T, Xu X. Recent advances in free energy calculations with a combination of molecular mechanics and continuum models. *Curr Comput Aided-Drug Des* 2006;2:287–306. <https://doi.org/10.2174/157340906778226454>
- [73] Zhang D, Lazim R. Application of conventional molecular dynamics simulation in evaluating the stability of apomyoglobin in urea solution. *Sci Rep* 2017 71 2017;7:1–12. <https://doi.org/10.1038/srep44651>
- [74] Zhou P, Yang XLou, Wang XG, Hu B, Zhang L, Zhang W, et al. A pneumonia outbreak associated with a new coronavirus of probable bat origin. *Nature* 2020;579:270–3. <https://doi.org/10.1038/s41586-020-2012-7>
- [75] Fusani L, Palmer DS, Somers DO, Wall ID. Exploring ligand stability in protein crystal structures using binding pose metadynamics. *J Chem Inf Model*

- 2020;60:1528–39. https://doi.org/10.1021/ACS.JCIM.9B00843/SUPPL_FILE/C19B00843_SI_002.TXT
- [76] Allegra M, Tutone M, Tesoriere L, Attanzio A, Culletta G, Almerico AM. Evaluation of the IKK β binding of indicaxanthin by induced-fit docking, binding pose metadynamics, and molecular dynamics. *Front Pharm* 2021;12:2400. <https://doi.org/10.3389/fphar.2021.701568/BIBTEX>
- [77] Yin Z. Mechanism of small molecules inhibiting activator protein-1 DNA binding probed with induced fit docking and metadynamics simulations. *J Chem Inf Model* 2019;59:5276–80. https://doi.org/10.1021/ACS.JCIM.9B00693/SUPPL_FILE/C19B00693_SI_005.ZIP
- [78] Clark AJ, Tiwary P, Borrelli K, Feng S, Miller EB, Abel R, et al. Prediction of protein-ligand binding poses via a combination of induced fit docking and metadynamics simulations. *J Chem Theory Comput* 2016;12:2990–8. https://doi.org/10.1021/ACS.JCTC.6B00201/SUPPL_FILE/CT6B00201_SI_002.ZIP
- [79] Chahal V., Kakkar R. A combination strategy of structure-based virtual screening, MM-GBSA, cross docking, molecular dynamics and metadynamics simulations used to investigate natural compounds as potent and specific inhibitors of tumor linked human carbonic anhydrase IX. <https://doi.org/10.1080/07391102.2022.2087736> 2022.